

FLARE: Feed-forward Geometry, Appearance and Camera Estimation from Uncalibrated Sparse Views

Shangzhan Zhang^{1,2*}Jianyuan Wang^{3*}Yinghao Xu^{4*†}Nan Xue²Christian Rupprecht³Xiaowei Zhou^{1†}Yujun Shen²Gordon Wetzstein⁴¹Zhejiang University²Ant Group³University of Oxford⁴Stanford University

Figure 1. We present FLARE, a feed-forward approach that simultaneously recovers high-quality poses, geometry and appearance from uncalibrated sparse views within **0.5s**. Our model excels in the scenarios with a camera circling around the subject, and also shows robust generalization to real-world casual captures, such as an indoor bedroom. In the central area below, we casually captured six random bedroom images with minimal overlap. Our method demonstrates high-quality geometry reconstruction even in this challenging case.

Abstract

We present FLARE, a feed-forward model designed to infer high-quality camera poses and 3D geometry from uncalibrated sparse-view images (i.e., as few as 2-8 inputs), which is a challenging yet practical setting in real-world applications. Our solution features a cascaded learning paradigm with camera pose serving as the critical bridge, recognizing its essential role in mapping 3D structures onto 2D image planes. Concretely, FLARE starts with camera pose estimation, whose results condition the subsequent learning of geometric structure and appearance,

optimized through the objectives of geometry reconstruction and novel-view synthesis. Utilizing large-scale public datasets for training, our method delivers state-of-the-art performance in the tasks of pose estimation, geometry reconstruction, and novel view synthesis, while maintaining the inference efficiency (i.e., less than 0.5 seconds). The project page and code can be found at: <https://zhanghe3z.github.io/FLARE/>

1. Introduction

Reconstructing 3D scenes from multi-view images is a fundamental problem with wide-ranging applications across computer vision, perception, and computer graphics. Traditionally, this task requires a large number of images and complex optimization procedures. In this work, we propose a feed-forward model, FLARE, which can estimate camera poses, geometry, and appearance from uncalibrated sparse views within 0.5 seconds. Our model excels in scenarios with a camera circling around the subject, and also shows robust generalization to real-world casual captures, such as an indoor bedroom. In the central area below, we casually captured six random bedroom images with minimal overlap. Our method demonstrates high-quality geometry reconstruction even in this challenging case.

*The first three authors contributed equally. †Corresponding author.

tional approaches typically solve this problem in two stages: first, estimating camera parameters using Structure-from-Motion (SfM) solvers [20, 56, 65], and then predicting dense depth maps by Multi-View Stereo (MVS) to achieve dense 3D reconstruction [57, 59]. Despite the significant success of the SfM-MVS paradigm over the past decades, it faces two key limitations. First, these methods rely heavily on handcrafted feature matching and are non-differentiable, preventing them from fully leveraging recent advancements in deep learning. Second, traditional SfM approaches struggle with sparse views and limited viewpoints, significantly restricting their applicability in real-world scenarios.

Recent efforts to tackle these issues have shown potential, but significant challenges remain. Optimization-based approaches like BARF [36] and NeRF--[81] jointly optimize camera poses and geometry, but they require a good initialization and suffer from poor generalization to novel scenes. Deep camera estimation methods [35, 50, 51, 60, 76, 98] treat sparse-view SfM as a camera parameter regression problem, yet struggle with accuracy and generalization. VGGsFm [77] improves this by incorporating multi-view tracking and differentiable bundle adjustment but falls short in providing dense geometry. DUST3R[80] and MAST3R [32] propose generating a two-view point map with pixel-wise geometry, but their reliance on post-optimization global registration is time consuming and often yields suboptimal results. PF-LRM [78] offers feed-forward reconstruction from four images, but its tri-plane representation [5] limits performance in large-scale scenes. While these methods have demonstrated promising advances in sparse-view settings, they still lack a comprehensive solution that combines scalability, accuracy, and efficiency in camera, geometry, and appearance estimation.

We present FLARE, a novel feed-forward and differentiable system that infers high-quality geometry, appearance, and camera parameters from uncalibrated sparse-view images. Direct optimization of these parameters from images often presents significant learning difficulties, frequently converging to sub-optimal solutions with distorted geometry and blurry textures. To address these challenges, we introduce a novel cascade learning paradigm that progressively estimates camera poses, geometry, and appearance, relaxing traditional requirements for 3D reconstruction such as dense image views, accurate camera poses, and wide baselines. Our cascade learning paradigm lies in decomposing the challenging optimization problem into sequential stages, using camera poses as proxies for each stage. The central concept is that a camera pose frames a 2D image within a 3D observation frustum, reducing the learning complexity for subsequent tasks. Our method starts with a neural pose predictor that estimates coarse camera poses from sparse-view images. These initial poses provide geometric cues that facilitate a transformer-based

architecture to refine the poses, compute point maps, and predict 3D Gaussians for novel-view synthesis. For geometry prediction, we introduce a two-stage approach instead of direct global prediction. First, we estimate camera-centric point maps in individual camera coordinates. Then, a neural scene projector unifies these local point maps into a coherent global structure. With this approach, we enable faster convergence in geometry learning and reduce geometric distortion for challenging scenes.

We trained our model on a set of large public datasets [1, 34, 39, 49, 68, 82, 92, 94]. FLARE achieves state-of-the-art results in camera pose estimation, point cloud estimation, and novel-view synthesis. With unposed images as input, FLARE can produce photorealistic novel-view synthesis using Gaussian Splatting in just 0.5 seconds, which is a substantial improvement over previous optimization-based methods. As demonstrated in Fig. 1, our system reconstructs 3D scenes and estimates poses from as few as 2-8 input images.

The primary contributions of this work are as follows:

- We propose an efficient, feed-forward, and differentiable system for high-quality 3D Gaussian scene reconstruction from uncalibrated sparse-view images, achieving inference in less than 0.5 seconds.
- We demonstrate that leveraging camera poses as proxies effectively simplifies complex 3D learning tasks. We thus introduce a novel cascaded learning paradigm that starts with camera pose estimation, whose results condition the subsequent learning of geometric structure and appearance.
- We propose a two-stage geometry learning approach that first learns camera-centric point maps and builds a global geometry projector to unify the point maps into a global coordinate.

2. Related Work

Structure-from-Motion (SfM). SfM techniques aim to estimate camera poses and reconstruct sparse 3D structures. Conventional approaches [56, 65] employ multi-stage optimization, starting with pairwise feature matching [2, 41, 43] across views to establish correspondences, followed by camera pose optimization using incremental bundle adjustment [71]. Recently, numerous learning-based SfM methods have been proposed to enhance the traditional multi-stage pipeline. These improvements focus on three main areas: developing learning-based feature descriptors [12, 13, 95], learning more accurate matching algorithms [54, 67], and implementing differentiable bundle adjustment [36, 75]. However, when input views are extremely sparse, accurately matching features becomes highly challenging, leading to degraded camera pose estimation performance.

Multi-view Stereo (MVS). MVS techniques aim to recon-

struct dense 3D geometry from multiple calibrated images. Traditional MVS methods [17, 18, 57] typically follow a pipeline of depth map estimation, depth map fusion, and surface reconstruction. These approaches often rely on photometric consistency across views and various regularization techniques [91] to handle challenging scenarios. Recent years have witnessed a surge in learning-based MVS methods, leveraging deep neural networks to improve reconstruction quality and efficiency either with cascade cost volume matching [90, 91] or reconstruction supervision with differentiable rendering [7, 8, 10, 23, 33, 85]. Despite significant progress, MVS methods consistently depend on calibrated camera poses, which are typically estimated by SfM methods. This cascaded pipeline often causes MVS to perform suboptimally when the estimated poses are inaccurate. DUS3R [32, 80] directly predicts the geometry of visible surfaces without any explicit knowledge of the camera parameters. However, under multi-view settings, their approach is limited to pairwise image processing followed by global alignment, failing to fully exploit multi-view information and supporting photorealistic rendering.

3D Reconstruction from Sparse-view Images. Neural representations [44, 45, 47, 61, 69] present a promising foundation for scene representation and neural rendering. When applied to novel-view synthesis, these methods have demonstrated success in scenarios with dense-view training images, showcasing proficiency in single-scene overfitting. Notably, recent advancements [9, 10, 24, 37, 40, 79, 96, 99] have extended these techniques to operate with a sparse set of views, displaying improved generalization to unseen scenes. These methods face challenges in capturing multiple modes within large-scale datasets, resulting in a limitation to generate realistic results. Additional works [7, 23, 33, 85] further scale up the model and datasets for better generalization with NeRF or Gaussian Splatting. Unlike existing methods that rely on calibrated camera poses to supervise the neural network training, our approach can perform direct 3D reconstruction from uncalibrated images.

Pose-free Novel-view Synthesis. Recent research has made significant progress in novel-view synthesis from uncalibrated images. One line of research focuses on jointly optimizing camera poses and radiance fields from dense-view images. BARF [36], NeRF-- [81], and subsequent works [3, 26, 72] have advanced this approach. Several recent methods [14, 15, 30] have extended the 3D representation from NeRF to 3D Gaussians. Another research direction [28, 46, 52, 83] focuses on developing feed-forward novel-view synthesis for unposed images. SRT [53] proposes the first pose- and geometry-free framework for novel view synthesis, while LEAP [27] pioneers pose-free radiance field reconstruction by directly estimating scene geometry and radiance fields. FlowCam [63] and FlowMap [64] introduce 2D flow to enable unsupervised learning of

generalizable 3D reconstruction, though their performance degrades in sparse-view settings. PF-LRM [78] estimates camera poses by predicting point maps and solving a differentiable perspective-n-point (PnP) problem, but shows limited generalization to complex 3D scenes. PF3plat [22] achieves coarse alignment of 3D Gaussians by leveraging pre-trained models for monocular depth estimation and visual correspondence. Splatt3R [62] and NopoSplat [93] utilize DUS3R [80] or MAST3R [32] to predict point maps as proxy geometry and subsequently learn 3D Gaussians for sparse-view reconstruction. However, existing approaches are either restricted to two-view scenarios or produce suboptimal rendering results due to imperfect geometry estimates from DUS3R or MAST3R. Our work presents a differentiable system that simultaneously predicts camera parameters, geometry, and appearance, achieving superior generalization across diverse real-world scenes.

3. Method

FLARE uses point maps [80] as our geometry representation for two key advantages: their compatibility with neural networks and natural integration with 3D Gaussians for appearance modeling. As shown in Fig. 2, FLARE is feed-forward model to infer high-quality camera poses and 3D geometry from uncalibrated sparse-view images. Our solution is a cascaded learning paradigm that first estimates camera poses from sparse views and then leverages the estimates to guide the subsequent geometry and appearance learning. We present our neural pose predictor for sparse-view pose estimation in Sec. 3.1. With the pose estimates, we propose a two-stage learning paradigm for geometry estimation (Sec. 3.2). Given the estimated geometry, we develop a 3D Gaussian reconstruction head that enables high-quality appearance modeling for photorealistic novel view synthesis (Sec. 3.3). Finally, we detail the training objectives for the whole framework (Sec. 3.4).

3.1. Neural Pose Predictor

Traditional pose estimation methods rely on feature matching to find correspondences, but this often fails in sparse-view scenarios where images have limited overlapping regions. Inspired by previous deep camera estimation methods [76, 77], we drop the feature matching and formulate pose estimation as a direct transformation problem from image space to camera space using an end-to-end transformer model. Given the input images $\mathcal{I} = \{\mathbf{I}_i\}_{i=1}^N$, we first tokenize them into non-overlapping patches to obtain image tokens. We then initialize learnable camera latents $\mathcal{Q}_c = \{\mathbf{q}_i^{\text{coarse}}\}_{i=1}^N$. By concatenating the image patches with camera latents into a 1D sequence, we leverage a small decoder-only transformer, named “neural pose predictor” $\mathbf{F}_p(\cdot)$ to estimate the coarse camera poses $\mathcal{P}_c =$

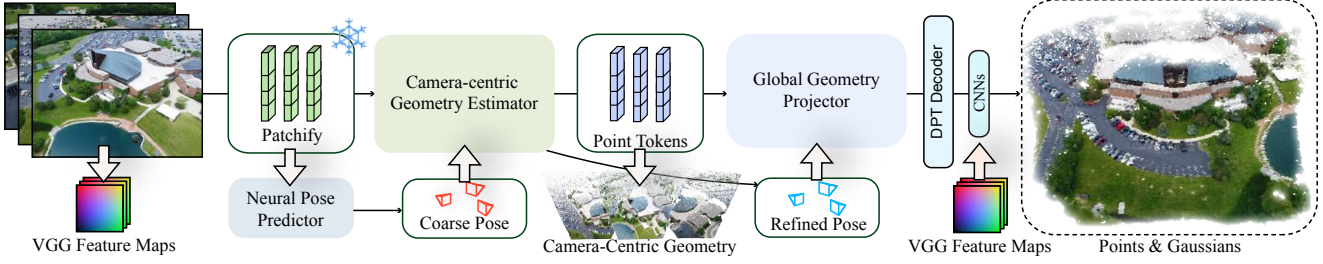


Figure 2. **Illustration of our pipeline.** Given uncalibrated sparse views, our model can infer high-quality camera poses, geometry and appearance in a single feed-forward pass. We use camera poses as proxies to guide subsequent geometry and appearance learning. Given initial pose estimates, we first compute camera-centric geometry, then project it into a global scene representation. Finally, we form 3D Gaussians on top of the scene geometry to enable photo-realistic novel-view synthesis.

$$\{\mathbf{p}_i^{\text{coarse}}\}_{i=1}^N: \quad \mathcal{P}_c = F_p(\mathcal{Q}_c, \mathcal{I}). \quad (1)$$

We parametrize each camera pose as a 7-dimensional vector comprising the absolute translation and a normalized quaternion. With this neural pose predictor, we can estimate coarse camera poses as initialization for subsequent geometry and appearance learning. We observe that the estimated poses do not need to be very accurate—only approximating the ground truth distribution is enough. This aligns with our key insight: camera poses, even imperfect, provide essential geometric priors and spatial initialization, which significantly reduces the complexity for geometry and appearance reconstruction.

3.2. Multi-view Geometry Estimation

With our estimated camera poses serving as an effective intermediate representation, we propose a two-stage geometry learning approach to improve reconstruction quality. Our key idea is to first learn camera-centric geometry in local frames (camera coordinate system) and then build a neural scene projector to transform it into a global world coordinate system with the guidance of estimated poses.

Camera-centric Geometry Estimation. Learning geometry in camera space aligns with the image formation process, as each view directly observes local geometry from its perspective. This also simplifies the geometry learning by focusing on local structures visible in each view, rather than reasoning about complex global spatial relationships. We tokenize images into image tokens and concatenate them with camera tokens derived from coarse pose estimates \mathcal{P}_c . These tokens are then fed into a transformer architecture $F_l(\cdot)$ to estimate local point tokens $\mathcal{T}_l = \{\mathbf{T}_i^{\text{local}}\}_{i=1}^N$. The self-attention mechanism in the transformer can perform association across different views and exploit the geometric cues from cameras. The local point tokens are subsequently fed into a DPT-based [48] decoder $D_l(\cdot)$ for spatial upsampling to obtain dense point maps $\mathcal{G}_l = \{\mathbf{G}_i^{\text{local}}\}_{i=1}^N$ and confidence map $\mathcal{C}_l = \{\mathbf{C}_i^{\text{local}}\}_{i=1}^N$ in local camera space. Meanwhile, we further refine the initial camera poses by

introducing additional learnable pose tokens \mathcal{Q}_f into the network, which output refined pose estimates \mathcal{P}_f alongside the geometry prediction:

$$\mathcal{T}_l, \mathcal{P}_f = F_l(\mathcal{I}, \mathcal{P}_c, \mathcal{Q}_f) \quad (2)$$

$$\mathcal{G}_l, \mathcal{C}_l = D_l(\mathcal{T}_l). \quad (3)$$

We can process an arbitrary number of images, as long as the GPU memory does not overflow. For a detailed explanation, please refer to the *supplementary materials*. We find this multi-task learning scheme can boost each task performance by providing complementary supervision signals between pose refinement and geometry estimation, as observed in previous work [78]. To handle potentially inaccurate pose estimates during inference, we introduce a simple yet effective pose augmentation strategy during training. Specifically, we randomly perturb the predicted camera poses by adding Gaussian noise, which allows the network to learn to adapt noisy estimated poses at inference time.

Global Geometry Projection. We aim to transform camera-centric geometry predictions into a consistent global geometry using refined camera poses. However, this transformation is challenging since imperfect pose estimates make direct geometric reprojection unreliable. Rather than using geometric transformation, we propose a learnable geometry projector $F_g(\cdot)$ that transforms local geometry \mathcal{G}_l into global space, conditioned on the estimated poses \mathcal{P}_f . This learned approach is more robust to pose inaccuracies compared to direct geometric projection. For computational efficiency, we utilize the local point tokens \mathcal{T}_l rather than the dense camera geometry \mathcal{G}_l as the input:

$$\mathcal{T}_g = F_g(\mathcal{T}_l, \mathcal{P}_f) \quad (4)$$

$$\mathcal{G}_g, \mathcal{C}_g = D_g(\mathcal{T}_g). \quad (5)$$

where $D_g(\cdot)$, \mathcal{G}_g and \mathcal{C}_g denotes the DPT-based upsampling decoder, global point maps and corresponding confidence map. This geometry projector $F_g(\cdot)$ is also implemented with a transformer architecture, which is the same as the $F_l(\cdot)$ but takes different input.

3.3. 3D Gaussians for Appearance Modeling

Based on the learned 3D point maps, we initialize 3D Gaussians by using the point maps as the centers of 3D Gaussians. We then build a Gaussian regression head to predict other Gaussian parameters including opacity $\mathcal{O} = \{\mathbf{o}_i\}_{i=1}^N$, rotation $\mathcal{R} = \{\mathbf{r}_i\}_{i=1}^N$, scale $\mathcal{S} = \{\mathbf{s}_i\}_{i=1}^N$ and spherical harmonics coefficient $\mathcal{SH} = \{\mathbf{sh}_i\}_{i=1}^N$ for appearance modeling. Specifically, to efficiently model appearance, we utilize a pretrained VGG network to extract features from input images $\mathcal{V} = \{\mathbf{v}_i\}_{i=1}^N$ and build another DPT head on top of the $\mathbf{F}_g(\cdot)$ to obtain an appearance feature \mathcal{A} . This appearance feature is then fused with VGG features and fed into a shallow CNN decoder $\mathbf{F}_a(\cdot)$ for Gaussian parameter regression.

To address scale inconsistency between estimated and ground truth geometry, we normalize both into a unified coordinate space. We compute average scale factors from predicted $s = \text{avg}(\mathcal{G}_g)$ and ground truth $s_{gt} = \text{avg}(\mathcal{G}_{gt})$ point maps, normalizing scenes to unit space during rendering. The Gaussian scale parameter \mathcal{S} and novel-view camera position \mathbf{p}' are also normalized. We use the differentiable Gaussian rasterizer $\mathbf{R}(\cdot)$ to render images with the normalized 3D Gaussians:

$$\mathbf{I}_{\mathbf{p}'} = \mathbf{R}(\{\mathcal{G}_g/s, \mathcal{O}, \mathcal{R}, \mathcal{S}/s, \mathcal{SH}\}, \mathbf{p}'/s_{gt}), \quad (6)$$

where $\mathbf{I}_{\mathbf{p}'}$ is the rendered image. The entire rendering process is differentiable, enabling end-to-end optimization of the Gaussian regression head through reconstruction loss.

3.4. Training Loss

Our model is a joint learning framework and trained with a multi-task loss function comprising three components: camera pose loss, geometry loss, and Gaussian splatting loss. The camera pose loss is defined as the combined sum of rotation and translation losses following the pose loss used in VGGSF:

$$\mathcal{L}_{\text{pose}} = \sum_{i=1}^N \ell_{\text{huber}}(\mathbf{p}_i^{\text{coarse}}, \mathbf{p}_i) + \ell_{\text{huber}}(\mathbf{p}_i^{\text{fine}}, \mathbf{p}_i), \quad (7)$$

where \mathbf{p}_i is the ground-truth camera pose of i -th image and ℓ_{huber} is the Huber-loss between the parametrization of poses.

The geometry loss includes a confidence-aware 3D regression term similar to that in DUS3R:

$$\mathcal{L}_{\text{geo}} = \sum_{i=1}^N \sum_{j \in \mathcal{D}^i} \mathbf{C}_{i,j}^{\text{camera}} \ell_{\text{regr}}^{\text{camera}}(j, i) - \alpha \log \mathbf{C}_{i,j}^{\text{camera}} \quad (8)$$

$$+ \sum_{i=1}^N \sum_{j \in \mathcal{D}^i} \mathbf{C}_{i,j}^{\text{global}} \ell_{\text{regr}}^{\text{global}}(j, i) - \alpha \log \mathbf{C}_{i,j}^{\text{global}}, \quad (9)$$

Table 1. **Comparison on multi-view pose estimation.** We compare our method to baselines using the RealEstate10K. We use RRA@5°, RTA@5° and AUC@30° to evaluate the pose accuracy.

Optimized-Based Method	RRA@5° ↑	RTA@5° ↑	AUC@30° ↑
DUS3R [80]	0.83	0.37	54.9
MAS3R [32]	0.87	0.45	61.1
COLMAP [55] + SPSG [54]	0.74	0.22	33.8
COLMAP [55]	0.63	0.07	16.0
PixSfM [38]	0.70	0.14	29.9
VGGSF [77]	–	–	72.1
RelPose [97]	0.47	0.32	11.1
Feed-forward Method	RRA@5° ↑	RTA@5° ↑	AUC@30° ↑
PoseDiffusion [76]	0.78	0.27	51.6
Ours	0.97	0.65	79.9

where \mathcal{D}^i denotes the valid pixel grids, $\mathbf{C}_{i,j}^{\text{local}}$ and $\mathbf{C}_{i,j}^{\text{global}}$ denote the confidence scores of pixel j of i -th image in local and global maps. $\ell_{\text{regr}}^{\text{local}}(j, i)$ and $\ell_{\text{regr}}^{\text{global}}(j, i)$ denote the Euclidean distances of pixel j of i -th image between the normalized predicted point maps and ground-truth point maps in camera and global coordinate frames.

The Gaussian splatting loss is computed as the sum of the L_2 loss and the VGG perceptual loss L_{perp} between the rendered $\mathbf{I}_{\mathbf{p}'}$ and ground truth $\hat{\mathbf{I}}_{\mathbf{p}'}$ images. Additionally, we include a depth loss to supervise rendered depth maps $\mathbf{D}_{\mathbf{p}'}$ with the prediction $\hat{\mathbf{D}}_{\mathbf{p}'}$ from the monocular depth estimator [88]:

$$\mathcal{L}_{\text{splat}} = \sum_{\mathbf{p}' \in \mathcal{P}'} \|\hat{\mathbf{I}}_{\mathbf{p}'} - \mathbf{I}_{\mathbf{p}'}\| + 0.5L_{\text{perp}}(\hat{\mathbf{I}}_{\mathbf{p}'}, \mathbf{I}_{\mathbf{p}'}) \quad (10)$$

$$+ 0.1\|(\mathbf{W}\hat{\mathbf{D}}_{\mathbf{p}'} + \mathbf{Q}) - \mathbf{D}_{\mathbf{p}'}\|, \quad (11)$$

where \mathbf{W} and \mathbf{Q} are the scale and shift used to align $\hat{\mathbf{D}}_{\mathbf{p}'}$ and $\mathbf{D}_{\mathbf{p}'}$, \mathcal{P}' is the novel-view camera poses.

The total loss is represented as:

$$\mathcal{L}_{\text{total}} = \lambda_{\text{pose}} \mathcal{L}_{\text{pose}} + \lambda_{\text{geo}} \mathcal{L}_{\text{geo}} + \lambda_{\text{splat}} \mathcal{L}_{\text{splat}}, \quad (12)$$

where λ_{pose} , λ_{geo} and λ_{splat} denotes the loss weight for corresponding loss.

4. Experiment

Datasets. Following DUS3R [80] and MAS3R [32], we train our model on a mixture of the following public datasets: MegaDepth [34], ARKitScenes [1], Blended MVS [92], ScanNet++ [94], CO3D-v2 [49], Waymo [68], WildRGBD [82], and DL3DV [39]. These datasets feature diverse types of scenes.

Implementation details. Our model is trained from scratch using 8 views as input, without any pre-trained models, except for the encoder. The neural pose predictor $\mathbf{F}_p(\cdot)$ consists of 12 transformer blocks with channel width

Table 2. **Comparison on Sparse-view Reconstruction.** The evaluation requires models to estimate both camera poses and scene geometry in the challenging sparse-view setting. For scene geometry, we report accuracy, completeness, and overall Chamfer distance. We use the accuracy for AUC under 30° degrees for camera poses.

Methods	DTU				ETH3D				TUM RGBD			
	ACC. \downarrow	COMP. \downarrow	Overall \downarrow	AUC@ 30° \uparrow	ACC. \downarrow	COMP. \downarrow	Overall \downarrow	AUC@ 30° \uparrow	ACC. \downarrow	COMP. \downarrow	Overall \downarrow	AUC@ 30° \uparrow
DUSt3R	3.8562	3.1219	3.4891	9.5	0.4856	0.7114	0.5984	10.0	0.3228	0.4388	0.3808	23.0
MASt3R	4.2380	3.2695	3.7537	12.3	0.3417	0.3626	0.3522	9.9	0.2547	0.3074	0.2810	37.4
Spann3R	4.3097	4.5573	4.4335	-	1.1589	0.8005	0.9797	-	0.5031	0.4643	0.4837	-
Ours	3.5049	2.7254	3.1152	28.1	0.4787	0.5169	0.4978	15.3	0.2046	0.2050	0.2048	53.6

768. In cascade geometry estimation, our camera-centric geometry estimator $F_l(\cdot)$ and global geometry projector $F_g(\cdot)$ both use 12 transformer blocks with channel width 768. We use the Adam [31] optimizer with an initial learning rate of 1×10^{-4} , gradually decreasing to 1×10^{-5} . We train our model on 64 NVIDIA A800 GPUs for 200 epochs with an input resolution of 512×384 . The training takes approximately 14 days to complete. More implementation details are presented in the *supplementary materials*.

Inference. Our model, although trained with 8 views, generalizes well to scenarios ranging from as few as 2 views to as many as 25 views. We give a comprehensive study between performance and view numbers in *supplementary materials*.

4.1. Multi-view Pose Estimation

Dataset. Following PoseDiffusion [76], we evaluate the camera pose estimates on the RealEstate10K dataset [101]. We apply our method directly to the RealEstate10K dataset without fine-tuning, using 5 images as input following previous protocol.

Metrics. We evaluate pose accuracy on the RealEstate10K dataset [101] using three metrics [29, 76]: AUC, RRA, and RTA. The AUC metric computes the area under the accuracy curve across different angular thresholds, where accuracy is determined by comparing the angular differences between predicted and ground-truth camera poses. RRA (Relative Rotation Accuracy) and RTA (Relative Translation Accuracy) measure the angular differences in rotation and translation respectively. The final accuracy at a threshold τ is determined by the minimum of RRA@ τ and RTA@ τ .

Baseline. For camera pose estimation, we compare our method with recent deep optimization-based methods, including DUSt3R [80], MASt3R [32], VGGsFm [77] and RelPose [97]. We also include traditional SfM methods such as COLMAP [55] and PixSfM [57], as well as feed-forward method PoseDiffusion [76].

Comparison. We show quantitative comparison in Tab. 1. Conventional SfM methods like COLMAP and PixSfM

rely on time-consuming bundle adjustment, resulting in slow inference speed for camera pose estimation. These optimization-based methods also struggle with sparse views where feature correspondences are difficult to establish. DUSt3R and MASt3R employ global alignment optimization, which not only leads to slow inference but also limits their performance due to their two-view geometry learning paradigm that cannot effectively leverage multi-view associations. Compared to other feed-forward approaches, our method achieves superior performance, thanks to the coarse-to-fine pose estimation strategy and multi-task learning with geometry.

4.2. Sparse-view 3D Reconstruction

Dataset. For sparse-view geometry reconstruction, we construct a comprehensive benchmark on the ETH3D [58], DTU [25], and TUM [66] datasets, which feature diverse scenes including objects, indoor scenes, and outdoor scenes.

Metrics and Baselines. We use the accuracy and completion metrics [25] to assess point cloud quality. We compare our method against recent state-of-the-art methods like DUSt3R [80], MASt3R [32], and Spann3R [74]. We also include conventional SfM methods like COLMAP [55] for comparison.

Comparison. As shown in Tab. 2, our method achieves higher performance than optimization-based methods like DUSt3R [80] and MASt3R [32], as well as recent feed-forward methods such as Spann3R [74]. Compared to DUSt3R and MASt3R, our method not only achieves better reconstruction quality but also offers faster inference, as our feed-forward reconstructor directly leverages multi-view information, avoiding their two-stage pipeline of two-view geometry estimation followed by global alignment post-processing. Our method also outperforms Spann3R by leveraging camera poses as geometric priors in our two-stage geometry learning paradigm, rather than directly regressing point maps through neural networks. We show qualitative comparisons in Fig. 3. Our model achieves better geometry reconstruction with less noise compared to other baselines.



Figure 3. **Qualitative Comparison results for sparse-view 3D reconstruction.** We visualize the 3D pointmaps of MASt3R [32], DUS3R [80], Spann3R [74] and our FLARE on ETH3D and TUM dataset.

Table 3. **Comparison of novel view rendering on the DL3DV.**

Method	PSNR \uparrow	SSIM \uparrow	LPIPS \downarrow
CoPoNeRF	16.06	0.472	0.474
pixelSplat	22.55	0.727	0.192
MVSplat	22.08	0.717	0.189
Ours (2 views)	23.04	0.725	0.182
Ours (8 views)	23.33	0.746	0.237

4.3. Novel-view Synthesis

Dataset. We evaluate rendering quality on two datasets: the RealEstate10K [101] and DL3DV [39]. For RealEstate10K, a widely used benchmark for novel view synthesis, we fine-tune our network using two-view images following the NopoSplat protocol [93], adding intrinsic as a condition. Since we focus on sparse views, our RealEstate10K tests only the results from the NopoSplat test split, specifically in the overlapping regions with low and medium overlap. For DL3DV, we sample 8 views for each testing video sequence as the input, and another 9 views as the groundtruth for evaluation. The sampling interval is randomly chosen, selected between 8 and 24. A total of 100 scenes are used as the test set.

Metrics and Baselines. To evaluate rendering quality in the RealEstate10K [101] and DL3DV [39] datasets, we employ PSNR, SSIM, and LPIPS metrics. To evaluate rendering quality, we compare with pose-free methods, including CoPoNeRF [21], Splatt3R, as well as pose-required methods, such as MVSplat [10] and PixelSplat [6]. We evaluate both MVSplat and pixelSplat using two-view inputs, selecting the two closest input views relative to the target view. Although MVSplat supports multiple input views, we find its performance degrades with additional views, as demonstrated in *supplementary materials*.

Table 4. **Comparison of novel view rendering on the RealEstate10k.** We evaluate all methods using 2 views.

Pose-required Method	PSNR \uparrow	SSIM \uparrow	LPIPS \downarrow
pixelNeRF	19.396	0.621	0.496
AttnRend	21.338	0.728	0.304
pixelSplat	22.495	0.777	0.210
MVSplat	22.568	0.781	0.200
Pose-free Method	PSNR \uparrow	SSIM \uparrow	LPIPS \downarrow
Splatt3R	15.113	0.492	0.442
CoPoNeRF	19.843	0.652	0.360
Ours	23.765	0.801	0.191

Comparison. Tab. 3 and Tab. 4 report the quantitative evaluation results for novel-view synthesis on DL3DV and RealEstate10K, respectively. Our approach substantially outperforms pose-free methods like CoPoNeRF [21] and Splatt3R [62], even better than the pose-required methods, including MVSplat [10] and PixelSplat [6] that take camera poses provided by the dataset to achieve high-fidelity rendering. Our model doesn’t require camera extrinsic information, which makes our method more applicable in real-world settings. Fig. 4 qualitatively illustrates that our pose-free method obtains higher rendering quality than the compared baselines.

4.4. Ablation Study

We conduct an ablation study to evaluate the effectiveness of each component in our method. For this study, we select the BlendedMVS [92] dataset. We randomly split the dataset of 95% scenes in BlendedMVS dataset as the training set and keep the rest 5% for testing. Our ablations exclude rendering loss to focus on geometric results with various design choices. “*w/o pose*” means our reconstructor is only conditioned on multiview images without inputting predicted camera poses. “*w/o camera-centric*” means that

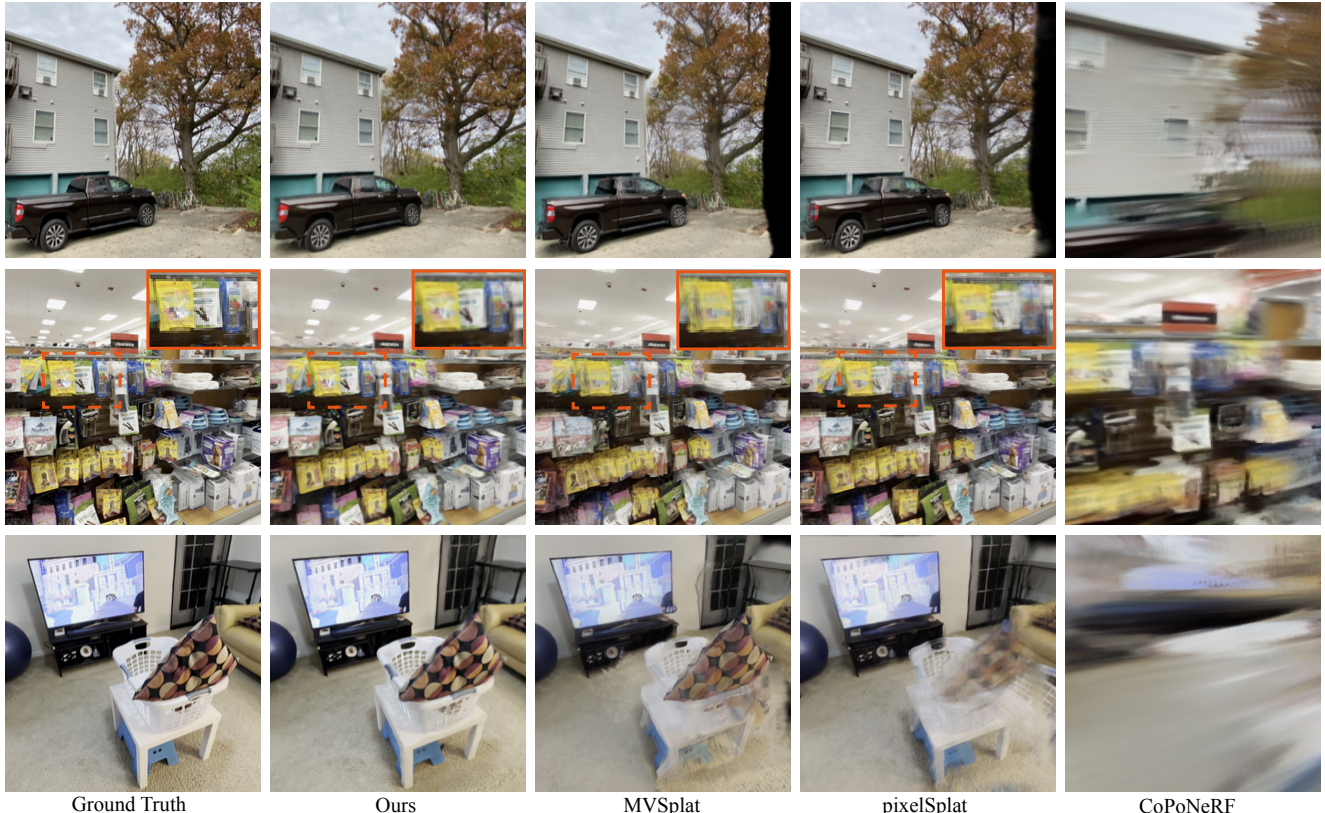


Figure 4. **Qualitative Comparison results for novel-view synthesis.** We visualize the rendering results from the DL3DV dataset, which shows that our method obtains high-quality rendering from sparse-view, uncalibrated input images.

we directly use a transformer with the same parameter size to output the global geometry without predicting camera-centric point maps. “w/o joint training” means first training the camera predictor separately and then fixing it while training the reconstructor. “w/o DPT head” denotes our ablation where we substitute the DPT decoder with a shallow MLP for point-map regression. “w/ rendering loss” refers to our configuration that incorporates rendering loss during training to evaluate its impact on geometric accuracy.

Table 5. **Ablation Study.** We evaluate the accuracy, completeness and the overall Chamfer distance on the testing set of Blended-MVS [92] for the learned geometry.

Method	ACC. \downarrow	COMP. \downarrow	Overall \downarrow
w/o DPT head	0.0399	0.0473	0.0436
w/o pose	0.0283	0.0356	0.0319
w/o camera-centric	0.0265	0.0326	0.0295
w/o joint training	0.0276	0.0322	0.0299
w/ rendering loss	0.0320	0.0244	0.0282
Ours	0.0250	0.0325	0.0288

As demonstrated in Tab. 5, using camera poses as proxies substantially improves geometry learning. Our two-stage approach with camera-centric geometry enhances performance, and the multi-task learning paradigm adds further improvements. DPT head plays a crucial role by explicitly accounting for spatial relationships during upsampling, whereas the shallow MLP lacks this consideration. The rendering loss has both positive and negative effects. While its dense supervision enhances COMP by supervising regions without ground truth point clouds, it slightly reduces ACC due to its lower accuracy compared to actual ground truth data.

5. Discussion

We introduce FLARE, a feed-forward model that can infer high-quality camera poses, geometry, and appearance from sparse-view uncalibrated images within 0.5 seconds. We propose a novel cascade learning paradigm that progressively estimates camera poses, geometry, and appearance, leading to substantial improvements over previous methods. Our model, trained on a set of public datasets, learns strong reconstruction priors that generalize robustly to challenging scenarios, such as very sparse views captured in real-world settings, enabling photo-realistic novel view synthesis.

Acknowledgements

We gratefully acknowledge Tao Xu for his assistance with the evaluation, Yuanbo Xiangli for insightful discussions, and Xingyi He for his Blender visualization code. This work was partially supported by NSFC (No. U24B20154), Zhejiang Provincial Natural Science Foundation of China (No. LR25F020003), Ant Group, and Information Technology Center and State Key Lab of CAD&CG, Zhejiang University.

References

- [1] Gilad Baruch, Zhuoyuan Chen, Afshin Dehghan, Tal Dimry, Yuri Feigin, Peter Fu, Thomas Gebauer, Brandon Joffe, Daniel Kurz, Arik Schwartz, et al. Arkitscenes: A diverse real-world dataset for 3d indoor scene understanding using mobile rgb-d data. *arXiv preprint arXiv:2111.08897*, 2021. [2](#) [5](#)
- [2] Herbert Bay, Tinne Tuytelaars, and Luc Van Gool. Surf: Speeded up robust features. In *Computer Vision–ECCV 2006: 9th European Conference on Computer Vision, Graz, Austria, May 7–13, 2006. Proceedings, Part I* 9, pages 404–417. Springer, 2006. [2](#)
- [3] Wenjing Bian, Zirui Wang, Kejie Li, Jia-Wang Bian, and Victor Adrian Prisacariu. Nope-nerf: Optimising neural radiance field with no pose prior. In *Proceedings of the IEEE/CVF Conference on Computer Vision and Pattern Recognition*, pages 4160–4169, 2023. [3](#)
- [4] Neill D. F. Campbell, George Vogiatzis, Carlos Hernández, and Roberto Cipolla. Using multiple hypotheses to improve depth-maps for multi-view stereo. In *ECCV*, 2008. [15](#)
- [5] Eric R Chan, Connor Z Lin, Matthew A Chan, Koki Nagano, Boxiao Pan, Shalini De Mello, Orazio Gallo, Leonidas J Guibas, Jonathan Tremblay, Sameh Khamis, et al. Efficient geometry-aware 3d generative adversarial networks. In *Proceedings of the IEEE/CVF conference on computer vision and pattern recognition*, pages 16123–16133, 2022. [2](#)
- [6] David Charatan, Sizhe Lester Li, Andrea Tagliasacchi, and Vincent Sitzmann. pixelsplat: 3d gaussian splats from image pairs for scalable generalizable 3d reconstruction. In *Proceedings of the IEEE/CVF Conference on Computer Vision and Pattern Recognition (CVPR)*, pages 19457–19467, 2024. [7](#)
- [7] David Charatan, Sizhe Lester Li, Andrea Tagliasacchi, and Vincent Sitzmann. pixelsplat: 3d gaussian splats from image pairs for scalable generalizable 3d reconstruction. In *Proceedings of the IEEE/CVF Conference on Computer Vision and Pattern Recognition*, pages 19457–19467, 2024. [3](#) [14](#)
- [8] Anpei Chen, Zexiang Xu, Fuqiang Zhao, Xiaoshuai Zhang, Fanbo Xiang, Jingyi Yu, and Hao Su. Mvsnerf: Fast generalizable radiance field reconstruction from multi-view stereo. In *Proceedings of the IEEE/CVF international conference on computer vision*, pages 14124–14133, 2021. [3](#)
- [9] Anpei Chen, Zexiang Xu, Fuqiang Zhao, Xiaoshuai Zhang, Fanbo Xiang, Jingyi Yu, and Hao Su. Mvsnerf: Fast generalizable radiance field reconstruction from multi-view stereo. In *Int. Conf. Comput. Vis.*, 2021. [3](#)
- [10] Yuedong Chen, Haofei Xu, Chuanxia Zheng, Bohan Zhuang, Marc Pollefeys, Andreas Geiger, Tat-Jen Cham, and Jianfei Cai. Mvsplat: Efficient 3d gaussian splatting from sparse multi-view images. *arXiv preprint arXiv:2403.14627*, 2024. [3](#) [7](#) [14](#)
- [11] Shuo Cheng, Zexiang Xu, Shilin Zhu, Zhuwen Li, Li Erran Li, Ravi Ramamoorthi, and Hao Su. Deep stereo using adaptive thin volume representation with uncertainty awareness. In *CVPR*, 2020. [15](#)
- [12] Daniel DeTone, Tomasz Malisiewicz, and Andrew Rabinovich. Superpoint: Self-supervised interest point detection and description. In *Proceedings of the IEEE conference on computer vision and pattern recognition workshops*, pages 224–236, 2018. [2](#)
- [13] Mihai Dusmanu, Ignacio Rocco, Tomas Pajdla, Marc Pollefeys, Josef Sivic, Akihiko Torii, and Torsten Sattler. D2-net: A trainable cnn for joint description and detection of local features. In *Proceedings of the ieee/cvf conference on computer vision and pattern recognition*, pages 8092–8101, 2019. [2](#)
- [14] Zhiwen Fan, Wenyan Cong, Kairun Wen, Kevin Wang, Jian Zhang, Xinghao Ding, Danfei Xu, Boris Ivanovic, Marco Pavone, Georgios Pavlakos, Zhangyang Wang, and Yue Wang. Instantssplat: Unbounded sparse-view pose-free gaussian splatting in 40 seconds, 2024. [3](#)
- [15] Yang Fu, Sifei Liu, Amey Kulkarni, Jan Kautz, Alexei A. Efros, and Xiaolong Wang. Colmap-free 3d gaussian splatting. In *Proceedings of the IEEE/CVF Conference on Computer Vision and Pattern Recognition (CVPR)*, pages 20796–20805, 2024. [3](#)
- [16] Yasutaka Furukawa and Jean Ponce. Accurate, dense, and robust multiview stereopsis. *PAMI*, 2010. [15](#)
- [17] Yasutaka Furukawa, Carlos Hernández, et al. Multi-view stereo: A tutorial. *Foundations and Trends® in Computer Graphics and Vision*, 9(1-2):1–148, 2015. [3](#)
- [18] Silvano Galliani, Katrin Lasinger, and Konrad Schindler. Massively parallel multiview stereopsis by surface normal diffusion. In *Proceedings of the IEEE international conference on computer vision*, pages 873–881, 2015. [3](#)
- [19] Silvano Galliani, Katrin Lasinger, and Konrad Schindler. Massively parallel multiview stereopsis by surface normal diffusion. In *ICCV*, 2015. [15](#)
- [20] Richard Hartley and Andrew Zisserman. *Multiple view geometry in computer vision*. Cambridge university press, 2003. [2](#)
- [21] Sunghwan Hong, Jaewoo Jung, Heeseong Shin, Jiaolong Yang, Seungryong Kim, and Chong Luo. Unifying correspondence, pose and nerf for pose-free novel view synthesis from stereo pairs. *arXiv preprint arXiv:2312.07246*, 2023. [7](#) [14](#)
- [22] Sunghwan Hong, Jaewoo Jung, Heeseong Shin, Jisang Han, Jiaolong Yang, Chong Luo, and Seungryong Kim. Pf3plat: Pose-free feed-forward 3d gaussian splatting. *arXiv preprint arXiv:2410.22128*, 2024. [3](#)

[23] Yicong Hong, Kai Zhang, Jiuxiang Gu, Sai Bi, Yang Zhou, Difan Liu, Feng Liu, Kalyan Sunkavalli, Trung Bui, and Hao Tan. Lrm: Large reconstruction model for single image to 3d. *arXiv preprint arXiv:2311.04400*, 2023. 3

[24] Ajay Jain, Matthew Tancik, and Pieter Abbeel. Putting nerf on a diet: Semantically consistent few-shot view synthesis. In *Int. Conf. Comput. Vis.*, 2021. 3

[25] Rasmus Jensen, Anders Dahl, George Vogiatzis, Engil Tola, and Henrik Aanæs. Large scale multi-view stereopsis evaluation. In *2014 IEEE Conference on Computer Vision and Pattern Recognition*, pages 406–413. IEEE, 2014. 6

[26] Yoonwoo Jeong, Seokjun Ahn, Christopher Choy, Anima Anandkumar, Minsu Cho, and Jaesik Park. Self-calibrating neural radiance fields. In *Proceedings of the IEEE/CVF International Conference on Computer Vision (ICCV)*, pages 5846–5854, 2021. 3

[27] Hanwen Jiang, Zhenyu Jiang, Yue Zhao, and Qixing Huang. Leap: Liberate sparse-view 3d modeling from camera poses. *ArXiv*, 2310.01410, 2023. 3

[28] Hanwen Jiang, Zhenyu Jiang, Kristen Grauman, and Yuke Zhu. Few-view object reconstruction with unknown categories and camera poses. *International Conference on 3D Vision (3DV)*, 2024. 3

[29] Yuhe Jin, Dmytro Mishkin, Anastasiia Mishchuk, Jiri Matas, Pascal Fua, Kwang Moo Yi, and Eduard Trulls. Image matching across wide baselines: From paper to practice. *International Journal of Computer Vision*, 129(2):517–547, 2021. 6

[30] Nikhil Keetha, Jay Karhade, Krishna Murthy Jatavallabula, Gengshan Yang, Sebastian Scherer, Deva Ramanan, and Jonathon Luiten. Splatam: Splat track & map 3d gaussians for dense rgb-d slam. In *Proceedings of the IEEE/CVF Conference on Computer Vision and Pattern Recognition*, pages 21357–21366, 2024. 3

[31] Diederik P Kingma. Adam: A method for stochastic optimization. *arXiv preprint arXiv:1412.6980*, 2014. 6

[32] Vincent Leroy, Yohann Cabon, and Jérôme Revaud. Grounding image matching in 3d with mast3r. *arXiv preprint arXiv:2406.09756*, 2024. 2, 3, 5, 6, 7, 15

[33] Jiahao Li, Hao Tan, Kai Zhang, Zexiang Xu, Fujun Luan, Yinghao Xu, Yicong Hong, Kalyan Sunkavalli, Greg Shakhnarovich, and Sai Bi. Instant3d: Fast text-to-3d with sparse-view generation and large reconstruction model. *arXiv preprint arXiv:2311.06214*, 2023. 3

[34] Zhengqi Li and Noah Snavely. Megadepth: Learning single-view depth prediction from internet photos. In *Proceedings of the IEEE conference on computer vision and pattern recognition*, pages 2041–2050, 2018. 2, 5

[35] Amy Lin, Jason Y Zhang, Deva Ramanan, and Shubham Tulsiani. Relpose++: Recovering 6d poses from sparse-view observations. *arXiv preprint arXiv:2305.04926*, 2023. 2

[36] Chen-Hsuan Lin, Wei-Chiu Ma, Antonio Torralba, and Simon Lucey. Barf: Bundle-adjusting neural radiance fields. In *Proceedings of the IEEE/CVF international conference on computer vision*, pages 5741–5751, 2021. 2, 3

[37] Kai-En Lin, Lin Yen-Chen, Wei-Sheng Lai, Tsung-Yi Lin, Yi-Chang Shih, and Ravi Ramamoorthi. Vision transformer for nerf-based view synthesis from a single input image. In *IEEE Winter Conf. Appl. Comput. Vis.*, 2023. 3

[38] Philipp Lindenberger, Paul-Edouard Sarlin, Viktor Larsson, and Marc Pollefeys. Pixel-Perfect Structure-from-Motion with Featuremetric Refinement. In *ICCV*, 2021. 5

[39] Lu Ling, Yichen Sheng, Zhi Tu, Wentian Zhao, Cheng Xin, Kun Wan, Lantao Yu, Qianyu Guo, Zixun Yu, Yawen Lu, Xuanmao Li, Xingpeng Sun, Rohan Ashok, Aniruddha Mukherjee, Hao Kang, Xiangrui Kong, Gang Hua, Tianyi Zhang, Bedrich Benes, and Aniket Bera. Dl3dv-10k: A large-scale scene dataset for deep learning-based 3d vision. In *Proceedings of the IEEE/CVF Conference on Computer Vision and Pattern Recognition (CVPR)*, pages 22160–22169, 2024. 2, 5, 7, 14

[40] Xiaoxiao Long, Cheng Lin, Peng Wang, Taku Komura, and Wenping Wang. Sparseneus: Fast generalizable neural surface reconstruction from sparse views. In *Eur. Conf. Comput. Vis.*, 2022. 3

[41] David G Lowe. Distinctive image features from scale-invariant keypoints. *International journal of computer vision*, 60:91–110, 2004. 2

[42] Zeyu Ma, Zachary Teed, and Jia Deng. Multiview stereo with cascaded epipolar raft. In *ECCV*, 2022. 15

[43] Jiri Matas, Ondrej Chum, Martin Urban, and Tomás Pajdla. Robust wide-baseline stereo from maximally stable extremal regions. *Image and vision computing*, 22(10):761–767, 2004. 2

[44] Lars Mescheder, Michael Oechsle, Michael Niemeyer, Sebastian Nowozin, and Andreas Geiger. Occupancy networks: Learning 3d reconstruction in function space. In *IEEE Conf. Comput. Vis. Pattern Recog.*, 2019. 3

[45] Ben Mildenhall, Pratul P Srinivasan, Matthew Tancik, Jonathan T Barron, Ravi Ramamoorthi, and Ren Ng. Nerf: Representing scenes as neural radiance fields for view synthesis. In *Eur. Conf. Comput. Vis.*, 2020. 3

[46] Bharath Raj Nagoor Kani, Hsin-Ying Lee, Sergey Tulyakov, and Shubham Tulsiani. Upfusion: Novel view diffusion from unposed sparse view observations. In *European Conference on Computer Vision (ECCV)*, 2024. 3

[47] Jeong Joon Park, Peter Florence, Julian Straub, Richard Newcombe, and Steven Lovegrove. Deepsdf: Learning continuous signed distance functions for shape representation. In *IEEE Conf. Comput. Vis. Pattern Recog.*, 2019. 3

[48] René Ranftl, Alexey Bochkovskiy, and Vladlen Koltun. Vision transformers for dense prediction. In *Proceedings of the IEEE/CVF international conference on computer vision*, pages 12179–12188, 2021. 4

[49] Jeremy Reizenstein, Roman Shapovalov, Philipp Henzler, Luca Sbordone, Patrick Labatut, and David Novotný. Common objects in 3d: Large-scale learning and evaluation of real-life 3d category reconstruction. *2021 IEEE/CVF International Conference on Computer Vision (ICCV)*, pages 10881–10891, 2021. 2, 5

[50] Chris Rockwell, Justin Johnson, and David F. Fouhey. The 8-point algorithm as an inductive bias for relative pose prediction by vits. In *3DV*, 2022. 2

[51] Chris Rockwell, Nilesh Kulkarni, Linyi Jin, Jeong Joon Park, Justin Johnson, and David F. Fouhey. Far: Flexible, accurate and robust 6dof relative camera pose estimation. 2024. 2

[52] Mehdi S. M. Sajjadi, Aravindh Mahendran, Thomas Kipf, Etienne Pot, Daniel Duckworth, Mario Lucic, and Klaus Greff. Rust: Latent neural scene representations from unposed imagery. In *2023 IEEE/CVF Conference on Computer Vision and Pattern Recognition (CVPR)*, pages 17297–17306, 2022. 3

[53] Mehdi S. M. Sajjadi, Henning Meyer, Etienne Pot, Urs Bergmann, Klaus Greff, Noha Radwan, Suhani Vora, Mario Lucic, Daniel Duckworth, Alexey Dosovitskiy, Jakob Uszkoreit, Thomas Funkhouser, and Andrea Tagliasacchi. Scene Representation Transformer: Geometry-Free Novel View Synthesis Through Set-Latent Scene Representations. *CVPR*, 2022. 3

[54] Paul-Edouard Sarlin, Daniel DeTone, Tomasz Malisiewicz, and Andrew Rabinovich. Superglue: Learning feature matching with graph neural networks. In *Proceedings of the IEEE/CVF conference on computer vision and pattern recognition*, pages 4938–4947, 2020. 2, 5

[55] Johannes Lutz Schöberger and Jan-Michael Frahm. Structure-from-motion revisited. In *Conference on Computer Vision and Pattern Recognition (CVPR)*, 2016. 5, 6

[56] Johannes L Schöberger and Jan-Michael Frahm. Structure-from-motion revisited. In *Proceedings of the IEEE conference on computer vision and pattern recognition*, pages 4104–4113, 2016. 2

[57] Johannes L Schöberger, Enliang Zheng, Jan-Michael Frahm, and Marc Pollefeys. Pixelwise view selection for unstructured multi-view stereo. In *Computer Vision–ECCV 2016: 14th European Conference, Amsterdam, The Netherlands, October 11–14, 2016, Proceedings, Part III* 14, pages 501–518. Springer, 2016. 2, 3, 6

[58] Thomas Schops, Johannes L Schöberger, Silvano Galliani, Torsten Sattler, Konrad Schindler, Marc Pollefeys, and Andreas Geiger. A multi-view stereo benchmark with high-resolution images and multi-camera videos. In *Proceedings of the IEEE conference on computer vision and pattern recognition*, pages 3260–3269, 2017. 6

[59] Steven M Seitz, Brian Curless, James Diebel, Daniel Scharstein, and Richard Szeliski. A comparison and evaluation of multi-view stereo reconstruction algorithms. In *2006 IEEE computer society conference on computer vision and pattern recognition (CVPR’06)*, pages 519–528. IEEE, 2006. 2

[60] Samarth Sinha, Jason Y Zhang, Andrea Tagliasacchi, Igor Gilitschenski, and David B Lindell. Sparsepose: Sparse-view camera pose regression and refinement. In *Proceedings of the IEEE/CVF Conference on Computer Vision and Pattern Recognition*, pages 21349–21359, 2023. 2

[61] Vincent Sitzmann, Michael Zollhöfer, and Gordon Wetzstein. Scene representation networks: Continuous 3d structure-aware neural scene representations. *Advances in Neural Information Processing Systems*, 32, 2019. 3

[62] Brandon Smart, Chuanxia Zheng, Iro Laina, and Victor Adrian Prisacariu. Splatt3r: Zero-shot gaussian splatting from uncalibrated image pairs. *arXiv preprint arXiv:2408.13912*, 2024. 3, 7

[63] Cameron Smith, Yilun Du, Ayush Tewari, and Vincent Sitzmann. Flowcam: training generalizable 3d radiance fields without camera poses via pixel-aligned scene flow. *arXiv preprint arXiv:2306.00180*, 2023. 3

[64] Cameron Smith, David Charatan, Ayush Tewari, and Vincent Sitzmann. Flowmap: High-quality camera poses, intrinsics, and depth via gradient descent. *arXiv preprint arXiv:2404.15259*, 2024. 3

[65] Noah Snavely, Steven M Seitz, and Richard Szeliski. Photo tourism: exploring photo collections in 3d. In *ACM siggraph 2006 papers*, pages 835–846, 2006. 2

[66] J. Sturm, W. Burgard, and D. Cremers. Evaluating egomotion and structure-from-motion approaches using the TUM RGB-D benchmark. In *Proc. of the Workshop on Color-Depth Camera Fusion in Robotics at the IEEE/RJS International Conference on Intelligent Robot Systems (IROS)*, 2012. 6

[67] Jiaming Sun, Zehong Shen, Yuang Wang, Hujun Bao, and Xiaowei Zhou. Loftr: Detector-free local feature matching with transformers. In *Proceedings of the IEEE/CVF conference on computer vision and pattern recognition*, pages 8922–8931, 2021. 2

[68] Pei Sun, Henrik Kretzschmar, Xerxes Dotiwalla, Aurelien Chouard, Vijaysai Patnaik, Paul Tsui, James Guo, Yin Zhou, Yuning Chai, Benjamin Caine, Vijay Vasudevan, Wei Han, Jiquan Ngiam, Hang Zhao, Aleksei Timofeev, Scott Ettinger, Maxim Krivokon, Amy Gao, Aditya Joshi, Yu Zhang, Jonathon Shlens, Zhifeng Chen, and Dragomir Anguelov. Scalability in perception for autonomous driving: Waymo open dataset. In *Proceedings of the IEEE/CVF Conference on Computer Vision and Pattern Recognition (CVPR)*, 2020. 2, 5

[69] Ayush Tewari, Justus Thies, Ben Mildenhall, Pratul Srinivasan, Edgar Tretschk, Wang Yifan, Christoph Lassner, Vincent Sitzmann, Ricardo Martin-Brualla, Stephen Lombardi, et al. Advances in neural rendering. In *Computer Graphics Forum*, pages 703–735. Wiley Online Library, 2022. 3

[70] Engin Tola, Christoph Strecha, and Pascal Fua. Efficient large-scale multi-view stereo for ultra high-resolution image sets. *Mach. Vis. Appl.*, 2012. 15

[71] Bill Triggs, Philip F McLauchlan, Richard I Hartley, and Andrew W Fitzgibbon. Bundle adjustment—a modern synthesis. In *Vision Algorithms: Theory and Practice: International Workshop on Vision Algorithms Corfu, Greece, September 21–22, 1999 Proceedings*, pages 298–372. Springer, 2000. 2

[72] Prune Truong, Marie-Julie Rakotosaona, Fabian Manhardt, and Federico Tombari. Sparf: Neural radiance fields from sparse and noisy poses. In *Proceedings of the IEEE/CVF Conference on Computer Vision and Pattern Recognition*, pages 4190–4200, 2023. 3

[73] Fangjinhua Wang, Silvano Galliani, Christoph Vogel, Pablo Speciale, and Marc Pollefeys. Patchmatchnet: Learned multi-view patchmatch stereo. In *CVPR*, pages 14194–14203, 2021. [15](#)

[74] Hengyi Wang and Lourdes Agapito. 3d reconstruction with spatial memory. *arXiv preprint arXiv:2408.16061*, 2024. [6](#), [7](#)

[75] Jianyuan Wang, Nikita Karaev, Christian Rupprecht, and David Novotny. Visual geometry grounded deep structure from motion. *arXiv preprint arXiv:2312.04563*, 2023. [2](#)

[76] Jianyuan Wang, Christian Rupprecht, and David Novotny. Posediffusion: Solving pose estimation via diffusion-aided bundle adjustment. In *Proceedings of the IEEE/CVF International Conference on Computer Vision*, pages 9773–9783, 2023. [2](#), [3](#), [5](#), [6](#)

[77] Jianyuan Wang, Nikita Karaev, Christian Rupprecht, and David Novotny. Vggsfm: Visual geometry grounded deep structure from motion. In *Proceedings of the IEEE/CVF Conference on Computer Vision and Pattern Recognition*, pages 21686–21697, 2024. [2](#), [3](#), [5](#), [6](#)

[78] Peng Wang, Hao Tan, Sai Bi, Yinghao Xu, Fujun Luan, Kalyan Sunkavalli, Wenping Wang, Zexiang Xu, and Kai Zhang. Pf-irm: Pose-free large reconstruction model for joint pose and shape prediction. *arXiv preprint arXiv:2311.12024*, 2023. [2](#), [3](#), [4](#)

[79] Qianqian Wang, Zhicheng Wang, Kyle Genova, Pratul P Srinivasan, Howard Zhou, Jonathan T Barron, Ricardo Martin-Brualla, Noah Snavely, and Thomas Funkhouser. Ibrnet: Learning multi-view image-based rendering. In *IEEE Conf. Comput. Vis. Pattern Recog.*, 2021. [3](#)

[80] Shuzhe Wang, Vincent Leroy, Yohann Cabon, Boris Chidlovskii, and Jerome Revaud. Dust3r: Geometric 3d vision made easy. In *Proceedings of the IEEE/CVF Conference on Computer Vision and Pattern Recognition*, pages 20697–20709, 2024. [2](#), [3](#), [5](#), [6](#), [7](#), [15](#)

[81] Zirui Wang, Shangzhe Wu, Weidi Xie, Min Chen, and Victor Adrian Prisacariu. Nerf: Neural radiance fields without known camera parameters. *arXiv preprint arXiv:2102.07064*, 2021. [2](#), [3](#)

[82] Hongchi Xia, Yang Fu, Sifei Liu, and Xiaolong Wang. Rgbd objects in the wild: Scaling real-world 3d object learning from rgb-d videos, 2024. [2](#), [5](#)

[83] Chao Xu, Ang Li, Linghao Chen, Yulin Liu, Ruoxi Shi, Hao Su, and Minghua Liu. Sparp: Fast 3d object reconstruction and pose estimation from sparse views. In *European Conference on Computer Vision*, pages 143–163. Springer, 2025. [3](#)

[84] Qingshan Xu and Wenbing Tao. Learning inverse depth regression for multi-view stereo with correlation cost volume. In *AAAI*, 2020. [15](#)

[85] Yinghao Xu, Zifan Shi, Wang Yifan, Hansheng Chen, Ceyuan Yang, Sida Peng, Yujun Shen, and Gordon Wetzstein. Grm: Large gaussian reconstruction model for efficient 3d reconstruction and generation. *arXiv preprint arXiv:2403.14621*, 2024. [3](#)

[86] Jianfeng Yan, Zizhuang Wei, Hongwei Yi, Mingyu Ding, Runze Zhang, Yisong Chen, Guoping Wang, and Yu-Wing Tai. Dense hybrid recurrent multi-view stereo net with dynamic consistency checking. In *European conference on computer vision*, pages 674–689. Springer, 2020. [14](#)

[87] Jiayu Yang, Wei Mao, José M. Álvarez, and Miaomiao Liu. Cost volume pyramid based depth inference for multi-view stereo. In *CVPR*, pages 4876–4885, 2020. [15](#)

[88] Lihe Yang, Bingyi Kang, Zilong Huang, Xiaogang Xu, Jiashi Feng, and Hengshuang Zhao. Depth anything: Unleashing the power of large-scale unlabeled data. In *CVPR*, 2024. [5](#)

[89] Yao Yao, Zixin Luo, Shiwei Li, Tian Fang, and Long Quan. Mvsnet: Depth inference for unstructured multi-view stereo. In *ECCV*, 2018. [15](#)

[90] Yao Yao, Zixin Luo, Shiwei Li, Tian Fang, and Long Quan. Mvsnet: Depth inference for unstructured multi-view stereo. In *Proceedings of the European conference on computer vision (ECCV)*, pages 767–783, 2018. [3](#)

[91] Yao Yao, Zixin Luo, Shiwei Li, Tianwei Shen, Tian Fang, and Long Quan. Recurrent mvsnet for high-resolution multi-view stereo depth inference. In *Proceedings of the IEEE/CVF conference on computer vision and pattern recognition*, pages 5525–5534, 2019. [3](#)

[92] Yao Yao, Zixin Luo, Shiwei Li, Jingyang Zhang, Yufan Ren, Lei Zhou, Tian Fang, and Long Quan. Blendedmvs: A large-scale dataset for generalized multi-view stereo networks. In *Proceedings of the IEEE/CVF conference on computer vision and pattern recognition*, pages 1790–1799, 2020. [2](#), [5](#), [7](#), [8](#)

[93] Botao Ye, Sifei Liu, Haofei Xu, Xuetong Li, Marc Pollefeys, Ming-Hsuan Yang, and Songyou Peng. No pose, no problem: Surprisingly simple 3d gaussian splats from sparse unposed images. *arXiv preprint arXiv:2410.24207*, 2024. [3](#), [7](#)

[94] Chandan Yeshwanth, Yueh-Cheng Liu, Matthias Nießner, and Angela Dai. Scannet++: A high-fidelity dataset of 3d indoor scenes. In *Proceedings of the IEEE/CVF International Conference on Computer Vision*, pages 12–22, 2023. [2](#), [5](#)

[95] Kwang Moo Yi, Eduard Trulls, Vincent Lepetit, and Pascal Fua. Lift: Learned invariant feature transform. In *Computer Vision–ECCV 2016: 14th European Conference, Amsterdam, The Netherlands, October 11–14, 2016, Proceedings, Part VI 14*, pages 467–483. Springer, 2016. [2](#)

[96] Alex Yu, Vickie Ye, Matthew Tancik, and Angjoo Kanazawa. pixelnerf: Neural radiance fields from one or few images. In *IEEE Conf. Comput. Vis. Pattern Recog.*, 2021. [3](#)

[97] Jason Y Zhang, Deva Ramanan, and Shubham Tulsiani. Relpose: Predicting probabilistic relative rotation for single objects in the wild. In *ECCV*, pages 592–611. Springer, 2022. [5](#), [6](#)

[98] Jason Y Zhang, Amy Lin, Moneish Kumar, Tzu-Hsuan Yang, Deva Ramanan, and Shubham Tulsiani. Cameras as rays: Pose estimation via ray diffusion. *arXiv preprint arXiv:2402.14817*, 2024. [2](#)

[99] Qihang Zhang, Shuangfei Zhai, Miguel Angel Bautista, Kevin Miao, Alexander Toshev, Joshua Susskind, and

Jiatao Gu. World-consistent video diffusion with explicit 3d modeling, 2024. 3

[100] Zhe Zhang, Rui Peng, Yuxi Hu, and Ronggang Wang. Geomvsnet: Learning multi-view stereo with geometry perception. In *CVPR*, 2023. 15

[101] Tinghui Zhou, Richard Tucker, John Flynn, Graham Fyffe, and Noah Snavely. Stereo magnification: Learning view synthesis using multiplane images. *arXiv preprint arXiv:1805.09817*, 2018. 6, 7

Appendix

In this supplementary material, we include: (1) extended implementation details covering data processing and training strategies, (2) additional experimental results, and (3) a comprehensive description of the network architecture.

A. Implementation Details

Data Processing. We follow the processing protocol of DUST3R to generate point maps for most datasets. However, the DL3DV dataset only provides the annotation for camera parameters. To include DL3DV into our training framework, we use the multi-view stereo algorithm from COLMAP to annotate per-frame depth maps, which are then converted into point maps. Additionally, we utilize multi-view photometric and geometric consistency to eliminate noisy depth [86]. For the datasets captured as video sequences, we randomly select 8 images from a single video clip, with each video clip containing no more than 250 frames. For multi-view image datasets, we randomly select 8 images per scene.

Baselines for Novel View Synthesis. We compare our novel view synthesis results with MVSplat [10], pixel-Splat [7], and CoPoNeRF [21] on the DL3DV dataset [39]. However, these methods were originally trained on only 2 views and perform not well under our sparse-view setting of 8 views. To ensure a fair comparison, we selected the two source views closest to the target rendering view as inputs for these baselines (e.g., MVSplat). We found that selecting two closest source views significantly improved their rendering quality compared to using all 8 views directly.

Numbers of Input Image. We have two camera latents: one for the first image (reference), and one is shared by all other images (source). The source token is duplicated $N-1$ times. Therefore, the model can process any number of input images.

B. Experiments

Relationship between MVSplat Performance and Input Views

We evaluated MVSplat with two views because its performance degrades with additional input frames, as shown in Fig. 5, as demonstrated in the figure above. We therefore reported its optimal results.

Study between Performance and the Number of Frames

We analyzed the impact of varying the number of frames on pose and point map estimation using the DTU dataset. For this experiment, we randomly selected 2, 6, 10, 16, and 25 source views while fixing two query views for testing pose

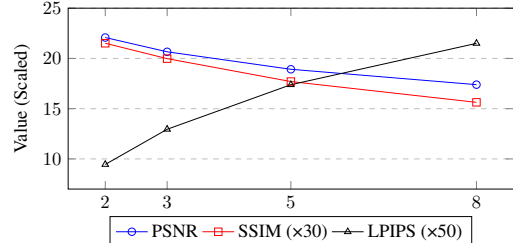


Figure 5. Relationship between MVSplat Performance and Input Views.

Table 6. Performance with a Varying Number of Input Frames. We study the impact of changing the number of input views on the performance of our method on the DTU dataset.

Metric	2 Views	6 Views	10 Views	16 Views	25 Views
AUC@30° \uparrow	59.09	70.45	80.15	81.52	81.81
ACC. \downarrow	4.07	2.79	0.94	0.24	0.30

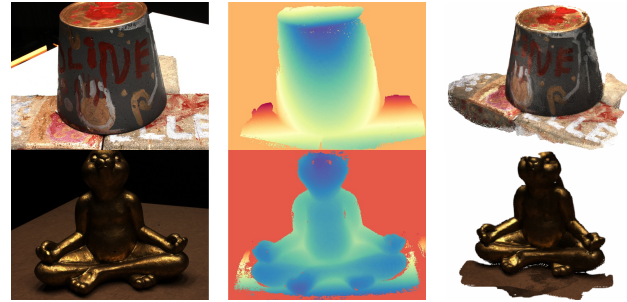


Figure 6. Qualitative Visualization of Sparse-view 3D Reconstruction on the DTU dataset. We visualize the input image (left), depth map (middle), and point cloud (right).

accuracy and for evaluating surface accuracy. Under the 2-view setting, our method generates a reasonable shape, but its precision remains limited. The results demonstrate that increasing the number of views leads to improvements in both pose and surface accuracy. However, these improvements gradually plateau as the number of views continues to grow, as shown in Tab. 6.

Dense View 3D Reconstruction on the DTU dataset

We present the results for dense view 3D reconstruction on the DTU dataset in Tab. 7, although dense reconstruction is not our primary objective. As observed, our method achieves better results compared to DUST3R but falls short of MAST3R. This is expected since our approach is not tailored for dense reconstruction, whereas MAST3R is specifically optimized for it through the training of matching heads.

Table 7. Dense View 3D Reconstruction on the DTU dataset.

We compare our method with baseline approaches using accuracy, completeness, and overall metrics under the dense view setting.

Methods	Accuracy↓	Completion↓	Overall↑
Camp [4]	0.835	0.554	0.695
Furu [16]	0.613	0.941	0.777
Tola [70]	0.342	1.190	0.766
Gipuma [19]	0.283	0.873	0.578
MVSNet [89]	0.396	0.527	0.462
CVP-MVSNet [87]	0.296	0.406	0.351
UCS-Net [11]	0.338	0.349	0.447
CER-MVS [42]	0.359	0.305	0.332
CIDER [84]	0.417	0.437	0.427
PatchmatchNet [73]	0.427	0.377	0.417
GeoMVSNet [100]	0.331	0.259	0.295
MAS3R [32]	0.403	0.344	0.374
DUSt3R [80]	2.677	0.805	1.741
Ours	1.932	0.715	1.321

Visualization of Sparse-view Reconstruction. We present the visualizations of our sparse-view reconstruction results on the DTU dataset in Fig. 6.